

# A real-space study of random extended defects in solids : application to disordered Stone-Wales defects in graphene.

Suman Chowdhury<sup>a</sup>, Santu Baidya<sup>b</sup>, Dhani Nafday<sup>b</sup>, Soumyajyoti Haldar<sup>d</sup>, Mukul Kabir<sup>c</sup>, Biplab Sanyal<sup>d</sup>, Tanusri Saha-Dasgupta<sup>b</sup>, Debnarayan Jana<sup>a</sup>, Abhijit Mookerjee<sup>b</sup>

<sup>a</sup>*Department of Physics, University of Calcutta, 92 Acharya Prafulla Chandra Road, Kolkata 700009, India*

<sup>b</sup>*Department of Condensed Matter and Materials Science, S. N. Bose National Centre for Basic Sciences, Block JD, Sector III, Salt Lake, Kolkata 700098, India*

<sup>c</sup>*Department of Physics, Indian Institute of Science Education and Research, Pune Sai Trinity Building, Pashan, Pune 411021, India*

<sup>d</sup>*Department of Physics and Astronomy, University of Uppsala, Uppsala, Sweden*

---

## Abstract

We propose here a first-principles, parameter free, real space method for the study of disordered extended defects in solids. We shall illustrate the power of the technique with an application to graphene sheets with randomly placed Stone-Wales defects and shall examine the signature of such random defects on the density of states as a function of their concentration. The technique is general enough to be applied to a whole class of systems with lattice translational symmetry broken not only locally but by extended defects and defect clusters. The real space approach will allow us to distinguish signatures of specific defects and defect clusters.

**Keywords:** Extended disordered defects, real space recursion method

**PACS:** 73.22.Pr; 63.22.Rc; 61.72.-y ; 46.35.+z

---

## 1. Introduction

The effect of random defects on the properties of solids is an important area in the study of materials. Defects are ubiquitous in solids [1]. Either formed naturally during their preparation or artificially engineered, they may profoundly affect their physical properties. Chemical reactions, phase transitions or plastic deformations during the formative stage may leave their imprints as defects. These defects may be local, like vacancies [2, 3], substitutional impurities [4] or adatoms [5]. Defects can also be extended, like dislocations, stacking faults, twins and grain boundaries. Extended defects have been visualized by STM images [6]. It is important therefore to set up a first-principles, essentially parameter free, theoretical methodology for the signature of random defects, and to distinguish, in particular, the role of disorder. Local random defects has been thoroughly studied using sophisticated mean-field approaches like the itinerant coherent potential approximation (ICPA) [7], the travelling cluster approximation (TCA)[8], both derived from the parent formalism : the augmented space formalism (ASF) [9, 10]. However, most of the work on extended defects have involved super-cell methods. These works look at essentially periodic arrays of defects with disorder stretching only over the finite super-cell [11–13]. Long ranged disorder is not accessible to these reciprocal space based methods. None of the supercell methods can accurately capture the disorder induced smearing of the density of states due to the self-energy arising out of scattering of Bloch waves by configuration fluctuations. This ‘life-time’ effect is experimentally accessible through neutron scattering and has been found to be strongly dependent both on the energy  $E$  and the wave-vector  $\vec{k}$ . In this work we shall propose a fully real space technique, where the structure and Hamiltonian of the relaxed defected lattice goes as an input into a recursive algorithm which gives us the electronic structure carrying the signatures of disorder. Although the

application will be to a specific problem, the method is general enough to be applied in any solid carrying random extended defects.

Electronic structure of low-dimensional solids with extended defects have been addressed earlier [11–13]. Let us quote Shirodkar and Waghmare [13] :

“Our work, along with other work [11, 12] has involved a *periodic array* of SW defects, whereas SW defects are *randomly distributed* in a real sample.”

The authors go on to remark that although this disorder may not affect the vibrational spectrum significantly, the electronic structure obtained from a periodic array of SW defects needs to be interpreted with care. Our real space recursion approach [42] makes no appeal to lattice translational symmetry and is thus ideal for studying topological disorder and its effect on electronic structure. The illustration of this point is the justification of our proposed methodology and the main focus of this communication.

## 2. The real space recursive algorithm

Early in the seventies Heine and co-workers introduced [41, 42] the recursion method based on a fully real space technique to deal with lattices without any translation symmetry. The essential inputs are the geometry of the lattice and a tight-binding, sparse Hamiltonian.

As an example, and in view of our later applications, let us look at a honeycomb lattice and map its vertices onto the set of positive integers. The mapping is not unique, but necessarily one-to-one (Fig.1). The geometry of the lattice is uniquely described by a connectivity matrix  $C(n, m)$  which gives us the  $m$ -th neighbour of the vertex labelled as  $n$ . The central panel of Fig.1 shows a model in which up to third neighbour overlaps are taken into account. The connectivity matrix is :

$$C(n, m) = \left( \begin{array}{c|cccc|cccccc|cccc} 1 & 2 & 3 & 4 & 5 & 6 & 7 & 8 & 9 & 10 & 11 & 12 & 13 \\ \hline 2 & 9 & 10 & 1 & 3 & 4 & 12 & 11 & \dots & \dots & 5 & 8 & \dots \\ 3 & 6 & 5 & 1 & 11 & 4 & 2 & 13 & \dots & \dots & 7 & 10 & \dots \\ 4 & 7 & 8 & 1 & 3 & 12 & 2 & 13 & \dots & \dots & 6 & 9 & \dots \\ \hline \dots & \dots & \dots & \dots & \dots & \dots & \dots & \dots & \dots & \dots & \dots & \dots & \dots \end{array} \right) \quad (1)$$

The tight-binding Hamiltonian can be written as :

$$H = \sum_n \sum_\alpha \epsilon_\alpha P_{n\alpha} + \sum_{n \neq m} \sum_{\alpha\beta} t_{\alpha\beta}(n - m) T_{n\alpha, m\beta} \quad (2)$$

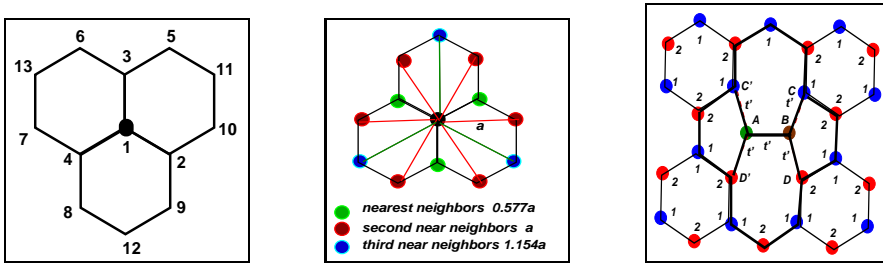


Figure 1: (Colour online) (left panel) The mapping of lattice sites on a honeycomb lattice onto a denumerable set of positive integers. (center) The nearest, next-nearest and third nearest neighbour vectors on a honeycomb lattice. (right panel) Lattice distortions and change in Hamiltonian elements around a structural defect.

Here,  $P$  and  $T$  are projection and transfer operators on the tight-binding basis labelled by  $n, \alpha$ , where  $n$  is the vertex label and  $\alpha$  all other possible degrees of freedom associated with it. Similarly, we describe a honeycomb lattice with a structural defect shown in the right most panel of Fig.1. We label the distorted sites say with a label  $\gamma$ , then whenever  $\alpha, \beta \neq \gamma$ ,  $t_{\alpha\beta}(n-m) = t(n-m)$  and otherwise  $t_{\alpha\beta}(n-m) = t'(n-m)$ .

With this recursion method, we shall study the representations of the Green operator or the resolvent of the Hamiltonian,

$$\mathbf{G}(z) = (z\mathbf{I} - \mathbf{H})^{-1}$$

where  $z$  is a complex variable. Most physically measurable quantities describing the electronic properties of a solid are related to different matrix elements of  $\mathbf{G}(z)$ . In particular, the local (atom projected) density of states (LDOS)  $n_i(E)$  and the total densities of states (TDOS)  $n(E)$  :

$$\begin{aligned} -\frac{1}{\pi} \lim_{z \rightarrow E - i0^+} \Im m G_{ii}(z) &= n_i(E) \\ -\frac{1}{\pi} \lim_{z \rightarrow E - i0^+} \frac{1}{N} \Im m \text{Tr } \mathbf{G}(z) &= n(E) \end{aligned} \quad (3)$$

Where  $N$  is the number of atoms in the system. It would be interesting to note that although the super-cell based methods can easily access both the band projected partial density of states (PDOS) and the total density of states (TDOS), it is only the real-space based methods that can give a single atom or an atomic cluster projected local densities of states (LDOS).

In this basis the representation of the Hamiltonian is a matrix of infinite rank. The solution of the Kohn-Sham equation of an electron in this system can be simplified enormously if the Hamiltonian has lattice translation symmetry. In that case the Bloch theorem introduces the quantum label  $\vec{k}$  and reduces the effectively infinite rank matrix representation of the Hamiltonian to a manageable finite rank equal to the number of bands (in this case two). Consequently, crystalline systems are always studied in this Bloch representation. But in disordered systems, particularly where the disorder is a topological distortion of the lattice and these defects are distributed randomly throughout it, such periodicity is absent and the reciprocal space representation is no longer strictly valid. In such situations we need to look for real-space based techniques.

Calculation of the resolvent requires inversion of a matrix of infinite rank. Haydock *et.al.* [41] proposed a technique to do so. We start from a suitable vertex at  $|1\rangle$ . It essentially involves generation of a new basis through a three term recurrence relation :

$$\begin{aligned} |1\rangle &= |n\alpha\rangle \\ |2\rangle &= (H - \alpha_1)|1\rangle \\ |n+1\rangle &= (H - \alpha_n)|n\rangle - \beta_{n+1}^2 |n-1\rangle \end{aligned} \quad (4)$$

$$\alpha_n = \frac{\langle n|H|n\rangle}{\langle n|n\rangle} \quad \text{and} \quad \beta_n^2 = \frac{\langle n|n\rangle}{\langle n-1|n-1\rangle} \quad (5)$$

Haydock *et.al.* [41] showed that the matrix element of the resolvent may be written as a continued fraction.

$$\langle n\alpha|G(z)|n\alpha\rangle = \{1|G(z)|1\} = \frac{1}{z - \alpha_1 - \frac{\beta_2^2}{z - \alpha_2 - \frac{\beta_3^2}{z - \alpha_3 - \frac{\beta_4^2}{\ddots z - \alpha_N - \beta_N^2 T(z)}}}} \quad (6)$$

Right at the start we emphasized that we have chosen a real space algorithm over mean-field and supercell approaches, because we do not wish to introduce artificial periodicity and confine randomness over a finite volume. But the problem with any numerical calculation is that we can deal with only a finite number of operations. In the recursion algorithm, we can go up to a finite number of steps leading to exactly what we wish to avoid. The analysis of the asymptotic part of the continued fraction then is of prime interest to us. This is the “termination” procedure in which the asymptotic behaviour is assessed from the way the coefficients  $\{\alpha_n, \beta_n\}$  behave as  $n \rightarrow \infty$ . Different terminators have been discussed in detail by Haydock and Nex [50], Luchini and Nex [51], Beer and Pettifor [52] and in considerable depth by Viswanath and Muller [53]. The terminator which describes the asymptotically far environment must satisfy certain basic properties : This termination process is a delicate mathematical approximation. We would like to maintain the Herglotz analytic properties of the resolvent after termination. A function  $T(z)$  is called Herglotz if :

- (i) All singularities of  $T(z)$  lie on the real  $z$ -axis.
- (ii) Singularities of  $T(z)$  form a bounded set.
- (iii)  $\text{Im } T(z) \geq 0$  if  $\text{Im } z < 0$  ;  $\text{Im } T(z) \leq 0$  if  $\text{Im } z > 0$ .
- (iv)  $\text{Re } T(z) \rightarrow 0$  as  $\text{Re } z \rightarrow \pm\infty$

The next step is to analyze our resolvent to locate singularities on its compact spectrum. Majority of resolvents with bounded spectra have singularities at the band edges. The termination of continued fractions describing spectral densities with compact support and singularities except at the band edges have been described in detail in earlier works [50–53].

The best illustration of this technique is to apply it to an interesting material where alternative methods always leads to problems of one sort or another. We have chosen to study graphene with random Stone-Wales defects.

### 3. The relaxed graphene lattice with random Stone-Wales defects.

In this work, we shall be interested in intrinsic extended structural defects like Stone-Wales (SW) defects [14] in graphene. The study of graphene, the two-dimensional allotrope of Carbon is an area of intense interest to both theoretical and experimental researchers for various reasons. The first is the possible technological applications of graphene[15–19]. Second, graphene seems to defy the theorem of Mermin and Wagner [20] and form a stable two-dimensional structure. Finally, the electrons in graphene behave like massless charged particles, something not encountered in our three dimensional world [21]. There has even been fanciful applications of general relativistic ideas in graphene. The SW defects are formed by  $90^\circ$  rotation of a C-C bond. After such a rotation, subsequent re-bonding leads to the formation of two pentagonal and two heptagonal carbon rings. This is illustrated in Fig. 2. These defects are responsible not only for bringing about fractures and embrittlement [22, 24–26], but also for altering the chemical reactivity and transport properties [27–29] and for causing the rippling behavior of graphene sheets [30]. SW defects can lead to out-of-plane displacement of carbon atoms in graphene[31–34] and induce

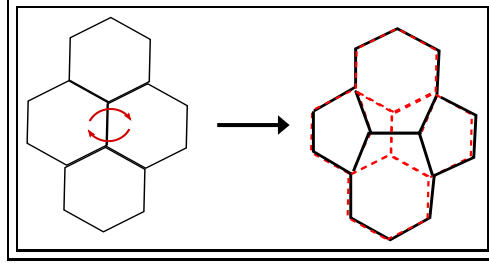


Figure 2: (Colour online) SW defect formation due to a  $\pi/2$  rotation of a C-C bond

curvature [35]. Recently, based on these three-dimensional ripples on the graphene sheets with SW defects, the assumption that SW defects are perfect two dimensional has been questioned [27, 28, 36–40].

For setting up the lattice model, we have started with a flat graphene sheet cluster, containing 3200 atoms. Different concentrations of Stone-Wales defects were then created by randomly choosing bonds on the lattice, rotating by  $\pi/2$  and rebonding as shown in Fig. 2. The first step of relaxations all lay on the graphene sheet and involved mainly on-plane relaxation of the C-atoms. The left panel in Fig.3 shows a vertical SW defect in the unrelaxed lattice while the right panel shows the effect of relaxation on the defect.

Lattice relaxation was carried out using the density functional tight binding method as implemented in a sparse-matrix based DFTB+ code [43]. In this method, a first-principles form of density functional is used and hence, large systems could be handled with reasonable accuracy. We have used the conjugate gradient method to relax the internal coordinates with  $10^{-2}$  eV/Å force convergence for the ionic relaxation and  $10^{-4}$  eV energy convergence for the electronic relaxation. Geometry optimizations were done using calculations at the  $\Gamma$  point in the Brillouin zone (BZ). The Fermi smearing method has been used with an electron temperature of 100K.

This relaxation first causes the rotated C-C bond length to compress to 1.32Å from its unrelaxed value of 1.44Å. As a consequence of this shortening of bond length, the bond angle at the apex of the pentagon compresses from 140 degree to 115 degree, which is 18.5%. Because of these large changes the system experiences a compressive stress along the direction of unrotated C-C bonds, and tensile stress along the rotated C-C bond. The graphene sheet then reduces this in plane stress by buckling in the z-direction, forming a non-planar, rippled structure. On structure relaxation the system energy is lowered.

Once the in-plane relaxation was completed we went a step further and relaxed the lattice in full three dimensions, allowing movement of atoms perpendicular to the original graphene plane. The top left panel of Fig. 4 shows the rippling of the graphene sheet on a single SW defect. The other three panels show rippling in a sheet with higher concentrations of SW-defect. Full lattice relaxation is thus extremely important for the structural changes

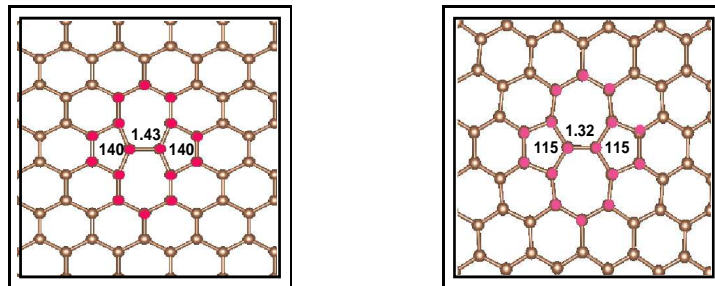


Figure 3: (Left) A vertical SW defect in the unrelaxed lattice (Right) The same defect after planar relaxation.

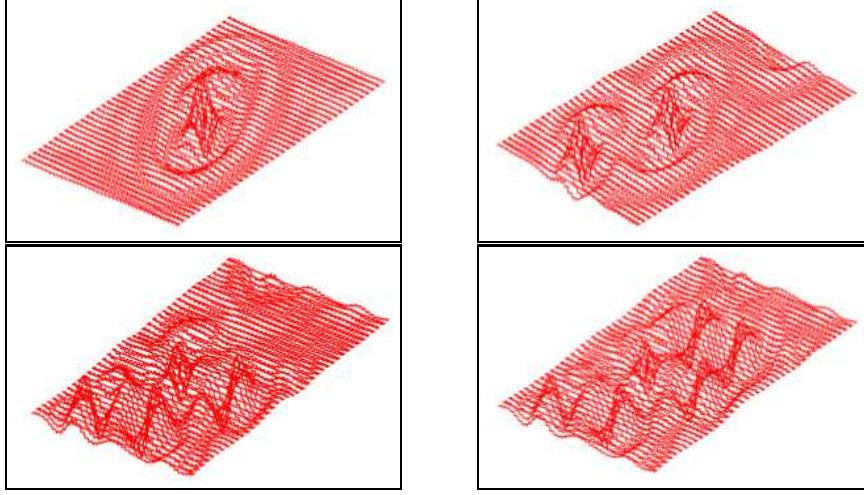


Figure 4: (Top, Left) Rippling of the graphene lattice on a single SW defect. (Top, Right and Bottom) Rippling of a graphene sheet with varying concentrations of SW-defects.

on relaxation may have very important effect on the electronic structure of the materials. We shall deal with the effects of structural changes with Harrison scaling[45, 46].

#### 4. First Principles derivation of the Hamiltonian.

Once we have constructed the relaxed graphene sheets with SW defects, the next step is to obtain a Hamiltonian for the band due to the  $\pi$ -bonded  $p_z$  electrons from first-principles, as far free from fitted parameters as possible. The calculations begin with a self-consistent ground state calculation for the single layer graphene using the tight-binding, linear muffin-tin orbitals (TBLMTO) method within the atomic sphere approximation. Three empty spheres were needed to achieve space filling. The muffin tin radii used for carbon (C) and the empty spheres were 1.56 a.u. and 2.76 a.u. respectively. The minimal basis set for the self-consistent calculation consisted of C  $s$ ,  $p_x$ ,  $p_y$ ,  $p_z$  and empty sphere  $s$  states. Fig.4 left panel shows the full TB-LMTO bands.

The *active orbitals* were recognized as the  $p_z$ . The remaining degrees of freedom were integrated out [44, 47] using a downfolding procedure. Formally, we partition the Hilbert space  $\mathcal{H}$  in which the Hamiltonian is defined

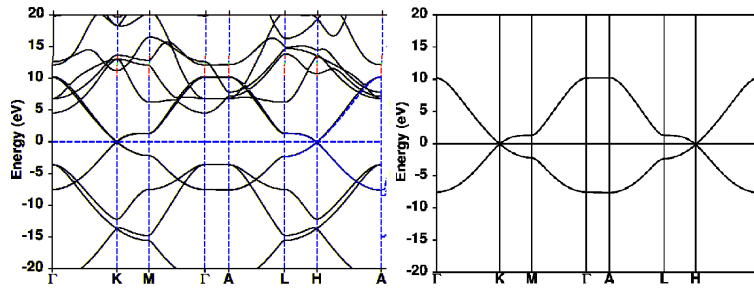


Figure 5: (Colour online) (Left panel) The TB-LMTO bands for pristine graphene (Right panel) The NMTO down-folded bands due to  $\pi$  bonding between the  $p_z$  states.

(eV)	$\varepsilon$	$t_1$	$t_2$	$t_3$
	-0.291	-2.544	1.668	-1.586

Table 1: Tight-binding parameters generated by NMTO.

into one which is spanned by the active orbitals  $\mathcal{H}_{\text{act}}$  and the rest, which we shall call the ‘bath’ :  $\mathcal{H} = \mathcal{H}_{\text{act}} \otimes \mathcal{H}_{\mathcal{B}}$  so that

$$H = \left( \begin{array}{c|c} H_{\text{act}} & H' \\ \hline H' & H_B \end{array} \right)$$

The partition or downfolding theorem gives the effective Hamiltonian in the subspace  $\mathcal{H}_{\text{act}}$  :

$$H_{\text{eff}} = H_{\text{act}} + H'^{\dagger} G_B(\varepsilon_n) H'$$

$G_B$  is calculated by inverting  $(\varepsilon_n I - H_B)$  in the bath subspace  $\mathcal{H}_B$ . For the present study, only the C- $p_z$  orbitals were kept active. All others including C-s,  $p_x$ ,  $p_y$  and empty sphere s-orbitals were downfolded. The integrated out orbitals renormalized the active C- $p_z$  orbital. The renormalized C- $p_z$  NMTOs were constructed using four energy mesh points  $\varepsilon_0$ -  $\varepsilon_3$  which gives 3<sup>rd</sup> order muffin tin orbitals. The energy mesh used for the construction of NMTOs were chosen to be in the energy window spanning the C- $p_z$  bands. The minimal set of C- $p_z$  NMTOs serve the purpose of effective localized C- $p_z$  Wannier functions.

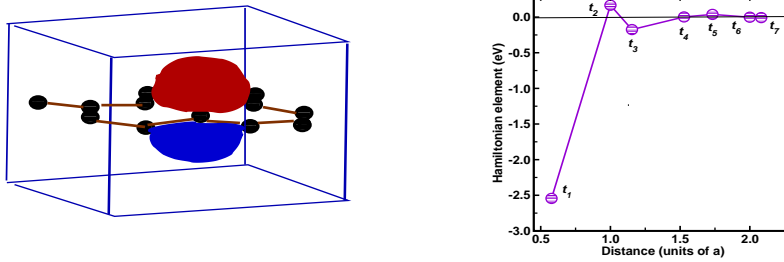


Figure 6: (Colour online) (Left)  $p_z$  orbitals perpendicular to the graphene plane. (Right) Hamiltonian parameters

The effective C- $p_z$  - C- $p_z$  hopping interaction:  $t(R, R')$ , connecting C- $p_z$  NMTO-s  $\chi(R)$  centered at the site  $R$  to the neighbouring C- $p_z$  NMTO  $\chi(R')$  centered at the  $R'$ , were obtained by Fourier transformation of the low energy C- $p_z$  Hamiltonian  $H_{p_z}(\vec{k})$  [47, 48]. These are shown in Fig.6 and Table 1.

The downfolded bands are shown on the top right panel of Fig.5. The corresponding  $t(R)$  is shown in the bottom right panel of Fig.5 and Table 1. Please note that the overlap is reasonably long ranged. Thus some of the earlier calculations with a simple nearest neighbour overlap (Reich *et.al.* [49]) may not show the accurate picture. Longer ranged overlap models have also been attempted. However, all of them are fitting procedures to the single C- $p_z$  bands. Our procedure of getting the bands from first-principles DFT calculations and then systematically down-folding away the non-active bands is both physically more appealing and mathematically more rigorous.

## 5. The Terminator

Having obtained the one band Hamiltonian (arising from the  $\pi$  bonded  $p_z$  orbitals), we carry out the recursion algorithm up to a finite number of steps. As discussed earlier, from the asymptotic behaviour of the recursion

coefficients we estimate the terminator. We analyze our resolvent to locate singularities on its compact spectrum. Majority of resolvents with bounded spectra have singularities at the band edges. The termination of continued fractions describing spectral densities with compact support and singularities on it have been described in detail in earlier works [50–53]. For graphene, we expect the  $\pi$  bands to have a spectral density which has an additional singularity at the Dirac point. Terminators appropriate to such problems have been discussed by Magnus [54] and Viswanath and Müller [53]. They propose a terminator of the form :

$$T(z) = \frac{2\pi(E_m)^{(\alpha+2\beta+1)/2}}{B\left(\frac{\alpha+1}{2}, 1+\beta\right)} |z - E_0|^\alpha \{(z - E_1)(E_2 - z)\}^\beta \quad (7)$$

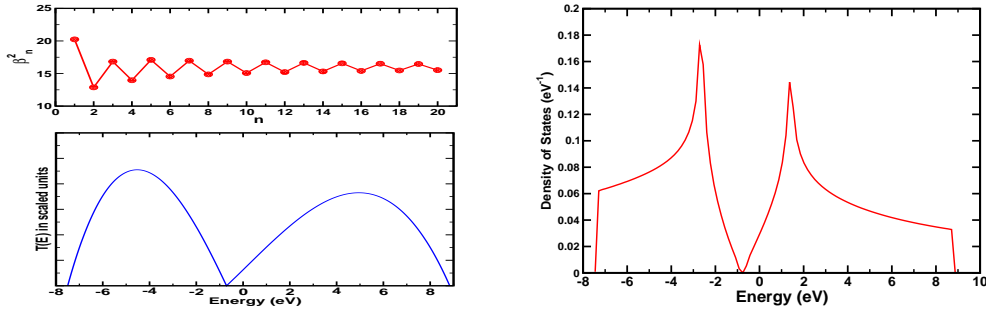


Figure 7: (Left,Top) The terminator with an internal singularity appropriate for graphene. (Left,bottom) Asymptotic parts of the calculated pristine graphene Green function continued fraction coefficients obtained by recursion. (Right) The TDOS of pristine graphene taking up to third nearest neighbour overlaps.

In our problem,  $E_0$  is the Dirac point and  $E_1, E_2$  are the spectral bounds,  $E_m^2 = E_1 E_2$ ,  $\alpha = \beta = 1$ .

Magnus [54] has cited a closed form for the continued fraction coefficients of the terminator :

$$\beta_{2n}^2 = \frac{4E_m^2 n(n+1)}{(4n+2)(4n+4)} \quad \beta_{2n+1}^2 = \frac{E_m^2 (2n+2)(2n+4)}{(4n+4)(4n+6)} \quad (8)$$

The parameters of the terminator are estimated from the asymptotic part of the continued fraction coefficients calculated for our problem. The top left panel in Fig.7 shows the continued fraction coefficients for the Viswanath-Muller terminator shown in the bottom left panel of this figure. The calculated continued fraction coefficients from recursion are shown in the right panel. The parameters of the terminator coefficients are fitted from these results. The resultant density of states is shown in the right panel of Fig.7. Unlike the usual nearest neighbour models the density is not symmetric round the Dirac point. If we write the Green function as contributions from non-intersecting paths (based on Feenberg perturbation [51]) then in the nearest neighbour model all non-intersecting paths are of even length and all  $\{\alpha_n\}$  is a constant, leading to a symmetric density. As soon as we introduce longer ranged  $t$ , odd length non-intersecting paths appear. Then  $\alpha_n$  vary with  $n$  and the density becomes non-symmetric.

## 6. Results and Discussion.

Since the axis of the SW defects are along the bond which is rotated in its formation, we note that the defects are either vertical or at angles  $60^\circ$  tilted to the left and right of the vertical. Closeups of two such isolated tilted defects are shown on the top row of Fig.8. We also show a double defect one tilted to the left and another to the right sharing a common hexagon. In the samples with higher concentrations of defects we also have clusters of connected defects. Two such examples of defect clusters are shown in the bottom row of Fig.8.



In order to analyze the signature of individual defects we first show the total density of states for several defect concentrations. This is shown in the top panels of Fig.9. We note that the occupied part of the spectrum below the Dirac point show very little change. The isolated defects show a defect state around 1 eV above the Dirac point. For the double defect this structure widens. There is also a defect induced signature around 3-4 eV above the Dirac point. These signatures were also observed by Shirodkar and Waghmare[13] (compare with their Fig. 5). Of course, in our real space picture there is no concept of defect ‘bands’, but the spectral signatures are very similar.

The supercell approaches indicate the local defect levels are very similar to our real space approach. However it has been known that the effect of the far disordered environment leads to a ‘self-energy’ [1], the real part of which shifts the defect levels and the imaginary part causes them to widen. In our continued fraction approach the terminator plays the role of the self-energy. As a result we clearly see the widening of the defect structures with increasing disorder. No periodic supercell technique can give this disorder broadening with accuracy. One added advantage of the real space approach is that we can focus of the atom or cluster projected local density of states and assign different signatures in the spectrum to particular isolated defects or defect clusters.

We propose that the real space recursion method is a powerful technique for the study of extended defects in disordered solids. Our application to random Stone-Wells defects in graphene justifies our proposal.

## Acknowledgements

SC would like to thank DST, India for financial support through the Inspire Fellowship. This work was done under the HYDRA collaboration between our institutes.

## References

- [1] J. Ziman, *Models of Disorder : The Theoretical Physics of Homogeneously Disordered Systems*, (Cambridge University Press, UK) (1979)
- [2] M.H. Gass, U. Bangert, A.L. Bleloch, P. Nair and A.K. Geim, *Nature Nanotechnology* 5 (2008) 676
- [3] J.C. Meyer, C. Kisielowski, R. Erni, M.D. Rosell, M.F. Crommie and A. Zettl, *Nano Letters* 8 (2008) 11
- [4] Y. Gan, L.Sun and F. Banhart, *Small* 4 (2008) 587

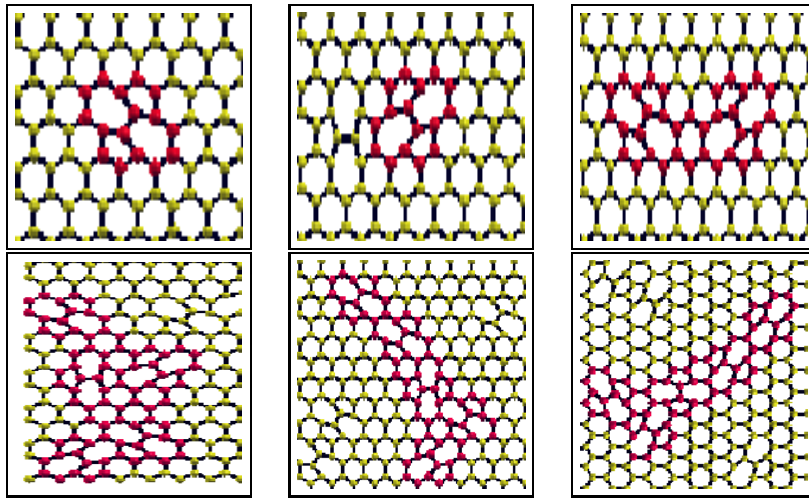


Figure 8: (Top panel) Single and connected double defects sharing a hexagon. (Bottom) Connected clusters of defects in systems with higher defect concentrations.

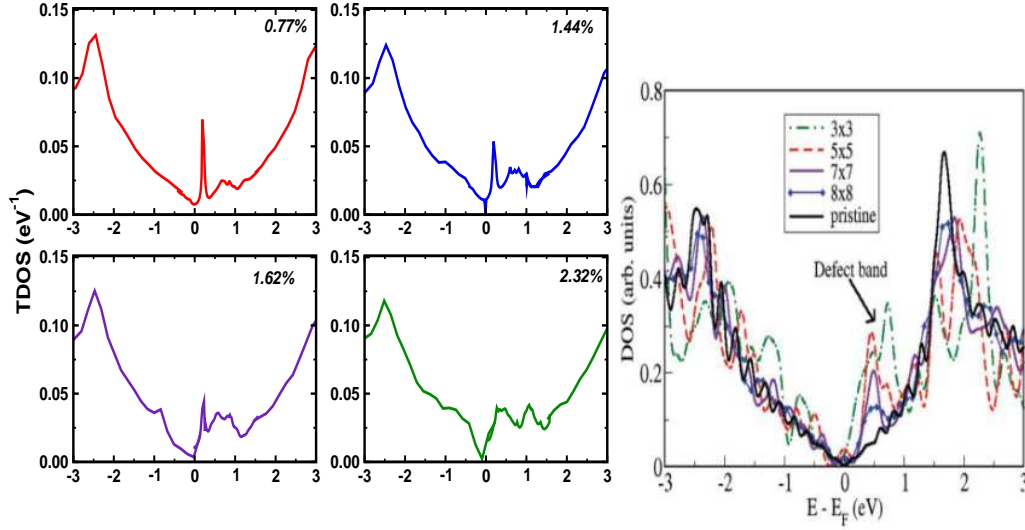


Figure 9: (Colour online) (Top) The total density of states near  $E_F$  for four different SW defect concentrations. (Bottom, left) The supercell results of Shirodkar and Waghmare.

- [5] J.C.Meyer, C.O. Girit, M.F. Crommie and A. Zettl, *Nature London* 454 (2008) 319
- [6] G.Y. Guo, B.C. Pan and L. Shi, *Physical Review B* 76 (2007) 155414
- [7] S. Ghosh, P.L. Leath and M.H. Cohen, *Physical Review B* 66 (2002) 214206
- [8] R. Mills and P. Ratanavararaksa, *Physical Review B* 18 (1978) 5291
- [9] A. Mookerjee, *Journal of Physics C : Solid State Physics* 6 (1973) L205
- [10] I. Dasgupta, T. Saha and A. Mookerjee, *Physical Review B* 51 (1995) 3413
- [11] X. Peng and R. Ahuja, *Nano Letters* 8 (2008) 4464
- [12] V.N. Popov, L. Henrard and P. Lambin, *Carbon* 47 (2009) 2448
- [13] S.N. Shirodkar and U. Waghmare, *Physical Review B* 86 (2012) 165401
- [14] A.J. Stone and D.J. Wales, *Chemical Physics Letters* 128 (1996) 501
- [15] A.H. Castro Neto, F. Guinea and N.M.R. Peres, *Physical Review B* 73 (2006) 205408
- [16] A.H. Castro Neto, F. Guinea and N.M.R. Peres, *Physics World* 19:11 (2006) 33
- [17] A.K. Geim and K. S. Novoselov, *Nature Materials* 6 (2007) 183
- [18] K. S. Novoselov, A.K. Geim, S.V. Morosov, D. Jiang, M.I. Katsnelson, I.V. Grigorieva, S.V. Dubonos and A.A. Firsov, *Nature London* 438 (2005) 197
- [19] Y. Zhang, T. Yan-wen, L.S. Horst and P. Kim, *Nature London* 438 (2005) 201
- [20] N.D. Mermin, *Physical Review B* 176 (1965) 250
- [21] J-N Fuchs and M.O. Goerbig, *Introduction to the Physical Properties of Graphene*, chapter 2 (2008)
- [22] B.R. Eggen, M.I. Heggie, G. Jungnickel, C.D. Latham, R. Jones and P.R. Briddon, *Science* 272 (1996) 87
- [23] C.P. Ewels, M.I. Heggie and P.R. Briddon, *Chemical Physics Letters* 351 (2002) 178
- [24] M.B. Nardelli, B.I. Yakobson and J. Bernholc, *Physical Review Letters* 81 (1998) 4656
- [25] M.B. Nardelli, B.I. Yakobson and J. Bernholc, *Physical Review B* 57 (1998) R4277
- [26] G.G. Samsonidze and B.I. Yakobson, *Physical Review Letters* 88 (2002) 065501
- [27] J. Kang, J. Bang, K. Ryu and K.J. Chang, *Physical Review B* 77 (2008) 115453
- [28] J. Carlsson and M. Scheffler, *Physical Review Letters* 96 (2006) 046806
- [29] D.W. Boukhvalov and M.I. Katsnelson, *Nano Letters* 8 (2008) 4373
- [30] I. Zsoldos, *Nanotechnology* 3 (2010) 101
- [31] S. Bhowmik and U.V. Waghmare, *Physical Review B* 81 (2010) 155416
- [32] E.J. Duplock, M. Schaeffler and P.J.D. Lindan, *Physical Review Letters* 92 (2004) 225502
- [33] F. OuYang, B. Huang, Z. Li, J. Xiao, H. Wang and H. Xu, *Journal of Physical Chemistry C* 12003 (2008)
- [34] Y. Zhao, R.E. Smalley and B.I. Yakobson, *Physical Review B* 66 (2002) 195409
- [35] H. Terrones and A.L. MacKay, *Carbon* 30 (1992) 1251

- [36] H. Amara, S. Latil, V. Meunier, P. Lambin and J-C Charlier, Physical Review B 76 (2007) 115423
- [37] G. Csányi, C.J. Pickard, B.D.Simons and R.J. Needs, Physical Review B 76 (2007) 115423
- [38] E. Kaxiras and K.C. Pandey, Physical Review Letters 61 (1988) 2693
- [39] L. Li, S. Reich and J. Robertson, Physical Review B 72 (2005) 184109
- [40] T. Lusk and L.D. Carr, Physical Review Letters 100 (2008) 175503
- [41] R. Haydock, V. Heine and M.J. Kelly, Journal of Physics C : Solid State Physics 5 (1972) 2845
- [42] V. Heine, Solid State Physics, ed. H. Ehrenreich and D. Turnbull, vol 35, chapter 1 (Academic Press, New York) (1990)
- [43] B. Aradi, B. Hourahine and Th Frauenheim, Journal of Physical Chemistry A111 (2007) 5678
- [44] O.K. Andersen and T. Saha-Dasgupta, Physical Review B 62 (2011) R16219
- [45] W.A. Harrison, Physical Review B 21 (1981) 5835
- [46] W.A. Harrison, Philosophical Magazine B 82 (2002) 1755
- [47] T. Saha-Dasgupta, A. Lichtenstein and R. Valenti, Physical Review B 71 (2004) 153108
- [48] H. Dreysee, Workshop LNP, volume 535 (1999) page 3
- [49] S. Reich, J. Maultzsch, C. Thomson and P. Ordejón, Physical Review B 66 (2002) 035412
- [50] R. Haydock and C.M.M. Nex, Physical Review B 74 (2006) 20521
- [51] M.U. Luchini and C.M.M.Nex, Journal of Physics C:Solid State Physics 20 (1987) 3125
- [52] N. Beer and D.G. Pettifor, Electronic Structure of Complex Systems, ed. P. Phariseau and W.M. Temmerman, volume 113 (1982) page 769 (Plenum Press, New York)
- [53] V.S. Viswanath and G. Müller, The User Friendly Recursion Method, Troisieme Cycle de la Physique en Suisse Romande (1993)
- [54] A. Magnus, The Recursion Method and its Applications, ed. D.G. Pettifor and D.L. Weire (Springer-Verlag, New York) (1987)